Laser-welded stainless steel I-sections: Residual stress measurements and column buckling tests

Gardner, Leroy; Bu, Yidu; Theofanous, Marios

DOI:
10.1016/j.engstruct.2016.08.057

Document Version
Peer reviewed version

Citation for published version (Harvard):
Gardner, L, Bu, Y & Theofanous, M 2016, 'Laser-welded stainless steel I-sections: Residual stress measurements and column buckling tests', *Engineering Structures*, vol. 127, pp. 536-548. https://doi.org/10.1016/j.engstruct.2016.08.057

Laser-welded stainless steel I-sections: Residual stress measurements and column buckling tests

Leroy Gardner [a], Yidu Bu [b,*], Marios Theofanous [c]

[a, b] Dept. of Civil and Environmental Engineering, Imperial College London, London, UK

[c] School of Civil Engineering, University of Birmingham, UK

[*] Corresponding author, Phone: +44 (0)20 7594 6058

Email: y.bu13@imperial.ac.uk

Abstract

Laser-welding is a high precision fabrication process suitable for joining a wide range of steels and stainless steels. Laser-welded structural stainless steel members, for which there are currently little experimental data owing to their recent introduction to the construction industry, are the focus of the present study. To address the lack of test data and to investigate their structural response, a total of 9 stub column tests and 22 flexural buckling tests (14 buckling about the minor axis and 8 about the major axis) have been performed on laser-welded austenitic stainless steel I-section members. Complementary tensile coupon tests, initial geometric imperfection measurements, and residual stress measurements have also been carried out and are reported herein. Based on the results obtained, a representative residual stress pattern is proposed, the design provisions of Eurocode 3 Part 1.4 and the continuous strength method are assessed, and column buckling curves for laser-welded stainless steel I-section members are recommended.

1. Introduction

Laser-welding is a high precision and efficient fabrication method used to locally melt and fuse together individual metallic elements of varying thicknesses and material grades into a range of complete structural sections, such as I-sections, T-sections, angles and channels, without the use of filler material. This technology can be used for the production of mild steel and stainless steel sections [1-3]. Laser-welding enables the heat input to be kept to a minimum, thus resulting in small heat affected zones, low thermal distortions and low residual stresses [2-4]. Compared to traditional arc welding, laser-welding offers the potential for a greater degree of automation, with higher welding speeds, quality and precision. The weld seams are also small in comparison to traditional arc welding processes, resulting in sections featuring essentially sharp edges and corners as shown in Fig. 1.

The structural response of laser-welded components has not received significant attention from researchers owing to their relatively recent introduction to the construction industry, and the applicability of current codes to their structural design is unclear. Experimental studies on laser-welded carbon steel cold-formed beams have been conducted [3], but no experimental data on the load-bearing performance of laser-welded stainless steel members have been reported to date. Given the importance of the fabrication process, and in particular the influence of residual stresses [5] on the structural response of members susceptible to buckling, there is a clear need for research into the behaviour and design of laser-welded members. To address the lack of relevant test data, a research project on laser-welded stainless steel sections comprising hot-rolled plated elements is underway at Imperial College London. This paper reports experimental results for austenitic stainless steel stub columns and long columns, covering 9 different geometries of laser-welded I-sections. Tensile coupon

tests, initial geometric imperfection measurements and residual stress measurements have also been conducted and are reported herein. Based on the results obtained, the design provisions of EN 1993-1-4 [6] and the continuous strength method are evaluated. EN 1993-1-4 [6] is found to be safely applicable to the design of laser-welded stainless steel cross-sections, but is overly conservative in the stocky range; this conservatism is overcome by application of the continuous strength method. Moreover, the suitability of the current buckling curve specified for welded sections in EN 1993-1-4 [6] is assessed for laser-welded profiles and it is concluded that higher column buckling curves than are currently prescribed for welded members may be adopted.

2. Material testing

The laser-welded I-section profiles investigated in this paper were fabricated from hot-rolled stainless steel plates. All tested material was austenitic stainless steel, but a variety of grades (Grades 1.4307, 1.4571 and 1.4404) was employed to suit the availability of sections from the manufacturer. These grades have similar mechanical properties and would therefore be expected to lead to similar structural performance. The laser-welding was carried out in accordance with EN ISO 13919-1 [7] with the quality level for weld imperfections being Class B (stringent). The longitudinal direction of the structural members coincided with the rolling direction of the constituent plate material.

The chemical compositions and key tensile properties of the plate material, as provided in the manufacturer's mill certificates, are reported in Tables 1 and 2, respectively, while the results of tensile coupon tests conducted in this study are presented in Table 3. Note that the material properties from the mill certificates are generally similar to those obtained from the tensile

coupon tests performed herein, though some variation exists. This may be due to differences in the location from which the coupon was extracted within the sheet and the loading direction (transverse to the rolling direction in the mill tests and longitudinal to the rolling (and member) direction for the tests performed herein), as well differences in testing apparatus, measurement equipment and loading rate. The adopted specimen designation system can be explained by means of an example – e.g. specimen I-160×82×10×12-W indicates an I-section of dimensions 160 (section height h) × 82 (section width b) × 10 (web thickness t_w) × 12 (flange thickness t_f), with the final letter (W=web; F=flange) indicating the component from which the coupon was extracted. The cross-section labelling system is shown in Fig. 2. All tensile coupon tests performed herein were conducted using an Instron 8802 250 kN hydraulic testing machine, following the procedure set out in EN ISO 6892-1 [8]. The reported material properties are Young's modulus E, 0.2% proof stress f_y, 1% proof stress $f_{1.0}$, ultimate tensile stress f_u, strain at ultimate stress ε_u, strain at fracture measured over the standard gauge length ε_f and the Ramberg-Osgood parameters n, $n_{0.2,1.0}$ and $n_{0.2,u}$ [9-12], which are measures of the degree of nonlinearity of the material response. The subscript 'mill' denotes that the properties were obtained from the manufacturer's mill certificate. For I-sections made up of plates of the same thickness t, a single coupon test was performed, while for sections made up of plates of dissimilar thicknesses, tensile tests on coupons extracted from both the flange (F) and the web (W) were conducted. As can be seen from the data in Tables 2 and 3, the tested austenitic stainless steel material exhibits high ductility, with strains at fracture in excess of 50% in most cases.

3. Residual stress measurements

As for conventional welding, the thermal gradients that arise during laser-welding lead to the formation of residual stresses. While the patterns and magnitudes of residual stresses in structural carbon steel cross-sections have been studied extensively [13, 14], those in stainless steel sections [5, 15, 16], particularly welded sections [17-20] have received less attention. Owing to the differences in material properties, such as a rounded stress-strain curve, higher thermal expansion and lower thermal conductivity, residual stresses in stainless steel sections cannot simply be assumed to be of the same magnitude or distribution as those in carbon steel sections. Moreover, the reduced heat input of laser-welding would be expected to result in lower thermal distortions and lower residual stresses compared to conventional processes.

The residual stress patterns in two laser-welded stainless steel cross-sections – I-140×140×10×12 (Grade 1.4307) and I-102×68×5×5 (Grade 1.4571) – were measured in the present study, using the sectioning method [5, 17, 21, 22]. The measured geometry of the residual stress test specimens is shown in Table 4, while the location and dimensions of the strips within the cross-section are set out in Fig. 3.

The residual stress measurements were made following the procedures recommended by the Structural Stability Research Council [23]. Prior to sectioning, the strips were marked out (see Fig. 3) and gauge holes were drilled in the middle of each end of the strip, using a CNC milling machine (see Fig. 4). The gauge holes were 1.98 mm in diameter, chamfered to a depth of 0.5 mm and cleaned with an air blast. The nominal initial distance between each pair of holes L_0 was set to 250 mm.

A Demec gauge was used to measure the distance between the gauge holes, following the recommendations of the Structural Stability Research Council [23]. Both strain gauges and

Demec gauges are considered to be acceptable and accurate means of measuring released strains following the sectioning process, and have been successfully employed and in fact compared in previous studies [5]. A Demec gauge was favoured in the present study to minimise the possibility of missing results that can arise due to loss of strain gauges during handling and machining. Readings were taken prior to (denoted r_1) and after (denoted r_2) the cutting procedure on both sides of the strips. A temperature reference bar was used to take into consideration any temperature changes; with readings taken prior to and after sectioning denoted t_1 and t_2, respectively.

All cutting was conducted using wire electrical discharge machining (EDM) with minimal heat input, as shown in Fig. 4. The two sectioned residual stress specimens are shown in Fig. 5. The residual stresses were obtained by calculating the relieved strain ε, according to Eq. (1):

$$\varepsilon = \frac{(r_2 - t_2) - (r_1 - t_1)}{L_0 + r_1 - t_1} \tag{1}$$

The expression above is such that positive strains indicate tensile residual stresses, and negative strains indicate compressive residual stresses.

Some of the released strips, particularly those close to the welds, exhibited a slight curvature in the longitudinal direction upon sectioning. This indicates a residual stress gradient through the thickness. To correct for this curvature and find the true relieved strain ε_c, the following approximation was applied [17]:

$$\varepsilon_c = \varepsilon + \frac{(\delta / L_0)^2}{6(\delta / L_0)^4 + 1} \tag{2}$$

in which δ is the maximum deviation of the strip from a straight line between the gauge points.

The residual stresses were then determined by multiplying the released strains by the Young's modulus. The resulting measured data are presented in Fig. 6, and show the anticipated pattern of tensile residual stresses near the welds and compressive residual stresses elsewhere, with some variation through the thickness. The higher through-thickness variation in residual stresses than is usually observed in welded sections may be related to a steeper through-thickness temperature gradient arising from the more localised heat input associated with laser-welding, though this is not consistent in the results and has not been verified. The normalised peak tensile and compressive residual stresses in the flanges and web of the two tested sections are reported in Table 5, where the subscripts f and w stand for flange and web, respectively, while t and c signify tension and compression, respectively. The measured residual stresses are also presented in a normalised format in Fig. 7, where positive values indicate tensile residual stresses and negative values indicate compressive residual stresses; in this figure, the residual stresses have been normalised by the tensile yield strength, while their locations have been normalised with respect to their position along the flanges and web, with 0.0 representing the web-to-flange junction and 1.0 representing the flange tip or web mid-point. Additional residual stress data obtained by Klopper et al. [19] on laser-welded stainless steel T-sections, together with the predictive model proposed in [17] for welded austenitic stainless steel sections are also plotted in the figure. Note that the measurements of Klopper et al. [18] are not directly comparable with those obtained herein since the test specimens were laser-welded from ferritic (Grade 1.4003) stainless steel plates. As anticipated, the measured residual stress magnitudes in the laser-welded sections are lower than those observed in sections produced using conventional welding techniques due to the lower heat input, and thus are over-predicted (see Fig. 7) by the model of Yuan et al. [17]. A revised pattern of representative residual stresses for laser-welded austenitic stainless steel cross-sections is therefore proposed herein based on the generic distribution adopted in [16],

but using the measurements obtained herein, as shown in Fig. 8. The model may be seen to provide generally safe-side predictions of the measured residual stress values. Note that although the peak tensile residual stresses obtained by Klopper et al. [18] are typically higher than those measured herein, the general distribution and the level of compressive residual stresses are similar. The values for the key parameters are set out in Table 6, together with those for equivalent predictive models for conventionally welded carbon steel [24, 25] and austenitic stainless steel [17] I-sections. The proposed residual stress pattern may be used in future numerical studies into the behaviour of laser-welded austenitic stainless steel structural elements.

4. Column tests

4.1 Stub columns

Stub column tests were conducted to assess the compressive response and susceptibility to local buckling of laser-welded I-sections. Stub column lengths equal to 3 times the largest cross-section dimensions (or 2 times the largest cross-section dimensions plus 254 mm, whichever is smaller) were chosen in accordance with the provisions of [23]. Similar recommendations are given in Annex A of EN 1993-1-3 [26]. This length is deemed long enough to contain a representative pattern of geometric imperfections and residual stresses, yet short enough to avoid overall member buckling. The ends of the stub columns were milled flat and square to ensure a uniform distribution of compressive force under load.

Prior to testing, the geometric properties of the stub columns specimens were measured and are recorded in Table 7. Initial local geometric imperfection measurements were also taken,

following the procedure reported in [27], to aid in the assessment of the structural behaviour and for use in the future development of numerical models. To measure the initial imperfections, the specimens were firstly secured to the flat bed of a milling machine. A displacement transducer, which was attached to the head of the milling machine, was then moved along a representative 600 mm length of each of the tested section sizes, recording displacements at 5 mm intervals along the locations shown in Fig. 9, where a typical local imperfection pattern is also depicted. The same approach has been successfully adopted in a previous study [28]. The maximum measured values of the local imperfections w_0, defined as the maximum deviation from a straight line datum fitted through each set of results, are reported in Table 7. The tolerances on web and flange deviations were taken as $(h\text{-}2t_f)/100$ and $b/100$, respectively, as set out in Annex D of EN 1090-2 [29]. The smaller of these two values, denoted $w_{0,tol}$, has been included in Table 7 for each cross-section size; on average, the measured local imperfections may be seen to be about one third of the EN 1090-2 tolerances.

The stub columns were compressed between parallel plates at a rate of 0.3 mm/min. Four strain gauges were affixed near the edges of the outer faces of the flanges at mid-height, whilst four LVDTs were employed to measure the end-shortening of the specimens. The strain gauge readings were utilized for alignment purposes and to account for the effect of the deformation of the end plates. All data, including voltage, load, strains and displacements were obtained through the DATASCAN data acquisition system at 1 second intervals. Each test was continued into the post-ultimate range to enable the post-failure response to be captured. All specimens failed by inelastic local buckling. The deformed stub column specimens, clearly displaying the local buckling failure modes, are depicted in Fig. 10. The load-end shortening responses are shown in Fig. 11, while the key measured geometric

properties and test results of the stub columns including the average measured compressive 0.2% proof strength f_{yc}, the recorded failure loads N_u and the corresponding end shortening at failure δ_u are reported in Table 7. The following notation is used: L is the stub column length, h is the overall cross-section height, b is the flange width, t_w is the web thickness, t_f is the flange thickness and w_0 is the measured local geometric imperfection amplitude.

4.2 Slender columns

4.2.1 Minor axis flexural buckling tests

Having established the basic material and cross-sectional response, fourteen flexural buckling tests on pin-ended columns buckling about the minor axis were conducted to obtain the ultimate load carrying capacity and assess the applicability of current buckling curves to the design of laser-welded I-section columns. Five cross-section sizes at various lengths were tested, covering a wide range of member slendernesses. Knife edges were employed to achieve the pin-ended conditions about the minor axis.

Prior to testing, the geometry of the specimens and the initial global geometric imperfections were measured and are reported in Table 8. The maximum global geometric imperfection of each column was determined by means of a self-levelling laser. The average measured global geometric imperfection magnitude v_0 was about L/6000 (i.e. significantly lower than the fabrication tolerance of L/750 set out in Annex D of EN 1090-2 [29]), but additional load eccentricity e_0 was applied such that a total eccentricity (v_0+e_0) of approximately L/1000 would result, where L is the buckling length of the columns between the knife edges (i.e. the sum of the column length and the thickness of the two knife edges).

The employed instrumentation consisted of a load cell at the top knife edge, two inclinometers attached at the top and bottom of the specimens to measure end rotations, one LVDT and one string potentiometer attached at the mid-height of the column to measure lateral deflections, as shown in Fig. 12. Four strain gauges (each at a distance of 10 mm from the outer edge of each flange) were affixed at the mid-height of the columns and used to determine the total test eccentricity (v_0+e_0) following the method described by Zhao et al.[30]. The average total applied eccentricity was L/1630. The discrepancy between the planned and the actual value of the applied eccentricity reflects the difficulty of accurately aligning the specimens. Load was applied by means of displacement-control at a rate of 1 mm/min for all tests. All data, including load, deflections and strain were recorded using the DATASCAN data acquisition system at 1 second intervals.

All specimens failed by flexural buckling around the minor axis, as shown by the typical deformed specimens in Fig. 13. The key experimental results are reported in Table 9, including ultimate load N_u, lateral displacement at ultimate load, and average end rotation at ultimate load. The measured load-lateral displacement responses for all specimens are shown in Fig. 14.

4.2.2 Major axis flexural buckling tests

Eight major axis flexural buckling tests on laser-welded I-sections columns were conducted following the same procedure as described in Section 4.2.1. Two sections sizes were tested, with different column lengths for each to achieve a spectrum of major axis member slenderness. Knife edges were employed to achieve pinned end conditions for buckling about

the major axis and fixed end conditions for buckling about the minor axis. Lateral restraints, preventing minor axis deflections, were provided to all specimens at quarter points, as shown along with the general test setup in Fig. 15. Similar to the minor flexural buckling tests, the geometric properties and global imperfections of the specimens were measured prior to testing and are reported in Table 10.

On average, the total applied eccentricity (v_0+e_0), as determined from the strain gauges, was *L*/785. All specimens failed by flexural buckling around the major axis, as depicted in Fig. 16 for three typical columns. The load-lateral deflection responses of all tested major axis buckling specimens are shown in Fig. 17, while the key experimental results are summarised in Table 11.

5. Analysis of results and design recommendations

5.1 Slenderness limits and cross-section response

The current European design code for stainless steel structures, EN 1993-1-4 [6], accounts for local buckling through the concept of cross-section classification. The constituent plate elements that make up the cross-section are classified into discrete behavioural groups according to their width-to-thickness ratios as compared to codified slenderness limits, which depend on the applied stress distribution, element support conditions (i.e. whether outstand or internal elements) and fabrication process (i.e. whether cold-formed or welded). The cross-section is assumed to behave according to its least favourably classified element. Based on the test results of the stub columns reported herein, the applicability of the Class 3

slenderness limits specified in EN 1993-1-4 for compressed outstand and internal elements in laser-welded cross-sections are assessed.

In Fig. 18, the experimentally derived ultimate loads from the tested stub columns, normalised by their compressive yield load Af_{yc}, are plotted against the element width-to-thickness ratio $c/t\varepsilon$ for both outstand and internal elements, where c is the flat width of the element, t is the thickness and $\varepsilon=[(235/f_{yc})(E/210000)]^{0.5}$. The EN 1993-1-4 Class 3 slenderness limits for internal and outstand elements, which were recently updated following research reported in [31], are also depicted. For the outstand flanges shown in Fig. 18(a), the tested range of $c/t\varepsilon$ ratios is rather limited and hence no clear conclusions can be drawn. However, for the internal elements in Fig. 18(b), it may be concluded that the EN 1993-1-4 limits are safely applicable to laser-welded cross-sections. It may also be observed that all tested sections exceeded their yield loads. This is attributed to the significant strain hardening exhibited by stocky stainless steel cross-sections, which is not accounted for in EN 1993-1-4 [6]. Strain hardening is however accounted for in the deformation based continuous strength method (CSM) [31-35]. Comparisons between the ultimate capacities obtained in the stub column tests N_u and the predicted capacities according to EN 1993-1-4 $N_{EN1993-1-4}$ and the CSM N_{csm} are presented in Table 12, where the benefit of considering strain hardening, in term of both mean predictions and reduction in coefficient of variation (COV), is clear.

5.2 Column buckling

EN 1993-1-1 [36] and EN 1993-1-4 [6] both specify different column buckling curves for different cross-section geometries and fabrication processes to reflect the range of geometric imperfections and residual stress patterns that they contain. Based on the experimental data

reported in [37], EN 1993-1-4 [6] specifies the use of buckling curve 'd' (with a plateau length $\bar{\lambda}_0$=0.20 and imperfection factor α=0.76) for welded stainless steel I-section columns buckling about the minor axis and buckling curve 'c' ($\bar{\lambda}_0$=0.20 and α=0.49) for buckling about the major axis. The experimental results reported herein are utilized to assess the suitability of these buckling curves for laser-welded stainless steel I-section columns. The buckling loads obtained from the tests are normalised by the compressive yield load Af_{yc}, as determined from the stub column tests similar to [38] and plotted against the non-dimensional member slenderness $\bar{\lambda} = \sqrt{Af_{yc} / N_{cr}}$ where N_{cr} is the elastic buckling load of the column, in Fig. 19. The figure also displays results from the tests on stainless steel I-section columns fabricated by conventional welding reported in [37] , as well as buckling curves 'c' and 'd'. The mean ratios of the predicted-to-test resistances ($N_{EN1993\text{-}1\text{-}4}/N_u$) are shown in Table 13. The following observations can be made: (i) the normalised results for the columns buckling about the minor axis are generally lower than those buckling about the major axis. This would be expected since the residual stress pattern in welded I-sections, where the outstand flange tips are in compression, is more detrimental to the minor axis flexural stiffness; (ii) the laser-welded sections generally exhibit superior normalised performance relative to their conventionally welded counterparts – this is attributed to the lower residual stress magnitudes, as discussed in Section 3; (iii) the comparisons indicate that curve 'c' may be suitable for laser-welded stainless steel columns buckling about either axis, but this should be verified by means of a further test or numerical data and reliability analysis, which is currently underway.

6. Conclusions

An experimental investigation into the structural response of laser-welded austenitic stainless steel I-section compression members has been reported. The study included tensile coupon

tests, initial geometric imperfection measurements, nine stub column tests, fourteen flexural buckling tests on pin-ended columns buckling about the minor axis and eight about the major axis. The level and distribution of residual stresses were assessed in two laser-welded austenitic stainless steel I-sections using the sectioning method, and a representative residual stress pattern for this section type was proposed. Following comparisons with the results of the stub column tests, the current Class 3 slenderness limit for internal elements given in EN 1993-1-4 [6], [31] was shown to be appropriate for laser-welded sections. The continuous strength method (CSM) was able to predict accurately the observed structural response of the tested stub columns by considering the influence of strain hardening. The results of the tests on the slender stainless steel laser-welded I-section columns indicated improved normalised buckling performance relative to conventionally welded sections due to the lower residual stress magnitudes and that a higher buckling curve may be applicable. The latter is being investigated further in a parallel numerical study and reliability analysis will be carried out on the combined experimental and numerical dataset.

Acknowledgements

The authors would like to thank Montanstahl AG for providing the test specimens and financial support for the project. The contribution of Gordon Herbert, Binhui Lin, Constantinos Kyprianou and Bartlomiej Drazyk in the experimental part of this research is gratefully acknowledged.

References

[1] Montanstahl AG. Laser Fusion. http://www.montanstahl.com/products/special-profiles/laser-fusion/. 2009.

[2] Shanmugam NS, Buvanashekaran G, Sankaranarayanasamy K, Kumar SR. A transient finite element simulation of the temperature and bead profiles of T-joint laser welds. Materials and Design. 2010;31:4528-42.
[3] Landolfo R, Mammana O, Portioli F, Di Lorenzo G, Guerrieri MR. Laser welded built-up cold-formed steel beams: Experimental investigations. Thin-Walled Structures. 2008;46:781-91.
[4] Majumdar D, Manna I. Laser material processing. International Materials Reviews. 2011;56:341-88.
[5] Cruise RB, Gardner L. Residual stress analysis of structural stainless steel sections. Journal of Constructional Steel Research. 2008;64:352-66.
[6] EN 1993-1-4:2006+A1:2015. Eurocode 3: Design of steel structures – Part 1.4: General rules supplmentary rules for stainless steels, including amendment A1 (2015). Brussels: European Committee for Standardization (CEN). 2015.
[7] EN ISO 13919-1. Welding: Electrons and laser beam welded joints – Guidance on quality levels for imperfections – Part 1: Steel. Brussels: European Committee for Standardization (CEN). 1997.
[8] EN ISO 6892-1. Metallic materials – Tensile testing – Part 1: Method of test at room temperature. Brussels: European committee for standardization (CEN). 2009.
[9] Mirambell E, Real E. On the calculation of deflections in structural stainless steel beams: an experimental and numerical investigation. Journal of Constructional Steel Research. 2000;54:109-33.
[10] Rasmussen KJR. Full-range stress-strain curves for stainless steel alloys. Journal of Constructional Steel Research. 2003;59:47-61.
[11] Gardner L, Nethercot DA. Experiments on stainless steel hollow sections - Part 1: Material and cross-sectional behaviour. Journal of Constructional Steel Research. 2004;60:1291-318.
[12] Arrayago I, Real E, Gardner L. Description of stress–strain curves for stainless steel alloys. Materials and Design. 2015;87:540-52.
[13] Nethercot DA. Residual stresses and their influence upon the lateral buckling of rolled steel beams. The Structural Engineer. 1974;52:89-96.
[14] Rasmussen K, Hancock G. Plate slenderness limits for high strength steel sections. Journal of Constructional Steel Research. 1992;23:73-96.
[15] Jandera M, Gardner L, Machacek J. Residual stresses in cold-rolled stainless steel hollow sections. Journal of Constructional Steel Research. 2008;64:1255-63.
[16] Young B, Lui W. Behavior of Cold-Formed High Strength Stainless Steel Sections. Journal of Structural Engineering. 2005;131:1738-45.
[17] Yuan HX, Wang YQ, Shi YJ, Gardner L. Residual stress distributions in welded stainless steel sections. Thin-Walled Structures. 2014;79:38-51.
[18] Gardner L, Cruise RB. Modeling of Residual Stresses in Structural Stainless Steel Sections. Journal of Structural Engineering. 2009;135:42-53.
[19] Klopper JJ, Laubscher RF, Steuwer A, James MN. An investigation into the effect of weld technique on the residual stress distribution of 3CR12 (DIN 1.4003) built-up structural sections. Proceedings of the Institution of Mechanical Engineers, Part L: Journal of Materials Design and Applications 2011;225:123-32.
[20] Lagerqvist O, Olsson A. Residual stresses in welded I-girders made of stainless steel and structural steel. Helsinki: Proceedings of the ninth nordic steel construction conference. 2001:737-44.
[21] Tebedge N, Alpsten G, Tall L. Residual-stress measurement by the sectioning method. Experimental Mechanics. 1973.
[22] Ma JL, Chan TM, Young B. Material properties and residual stresses of cold-formed high strength steel hollow sections. Journal of Constructional Steel Research. 2015;109:152-65.
[23] Ziemian RD. Guide to stability design criteria for metal structures: John Wiley & Sons; 2010.
[24] ECCS. European Convention for Constructional Steelwork: Convention Europeenne de la Construction Metallique. 1976.
[25] BSK99. Boverkets handbok om stalkonstruktioner, Swedish regulations for steel structures. 1999.
[26] EN 1993-1-3. Eurocode 3: Design of steel structures – Part 1.3: General rules – Supplementary rules for cold-formed members and sheeting. Brussels: European Committee for Standardization (CEN). 2006.
[27] Schafer BW, Pekoz T. Computational modeling of cold-formed steel: characterizing geometric imperfections and residual stresses. Journal of Constructional Steel Research. 1998;47:193-210.

[28] Saliba N, Gardner L. Cross-section stability of lean duplex stainless steel welded I-sections. Journal of Constructional Steel Research. 2013;80:1-14.
[29] EN 1090-2. Execution of steel structures and aluminium structures. Part 2: Technical requirements for steel structures. Brussels: European Committee for Standardization (CEN). 2011.
[30] Zhao O, Rossi B, Gardner L, Young B. Behaviour of structural stainless steel cross-sections under combined loading – Part I: Experimental study. Engineering Structures. 2015;89:236-46.
[31] Gardner L, Theofanous M. Discrete and continuous treatment of local buckling in stainless steel elements. Journal of Constructional Steel Research. 2008;64:1207-16.
[32] Afshan S, Gardner L. The continuous strength method for structural stainless steel design. Thin-Walled Structures. 2013;68:42-9.
[33] AISC Design Guide 27: Structural Stainless Steel. American Institute of Steel Construction (AISC), Chicago, Illinois, USA 2013.
[34] Ashraf M, Gardner L, Nethercot DA. Compression strength of stainless steel cross-sections. Journal of Constructional Steel Research. 2006;62:105-15.
[35] Buchanan C, Gardner L, Liew A. The continuous strength method for the design of circular hollow sections. Journal of Constructional Steel Research. 2016;118:207-16.
[36] EN 1993-1-1. Eurocode 3: Design of steel structures – Part 1.1: General rules and rules for buildings. Brussels: European Committee for Standardization (CEN). 2005.
[37] Burgan BA, Baddoo NR, Gilsenan KA. Structural design of stainless steel members comparison between Eurocode 3, Part 1.4 and test results. Journal of Constructional Steel Research. 2000;54:51-73.
[38] Theofanous M, Chan TM, Gardner L. Structural response of stainless steel oval hollow section compression members. Engineering Structures. 2009;31:922-34.

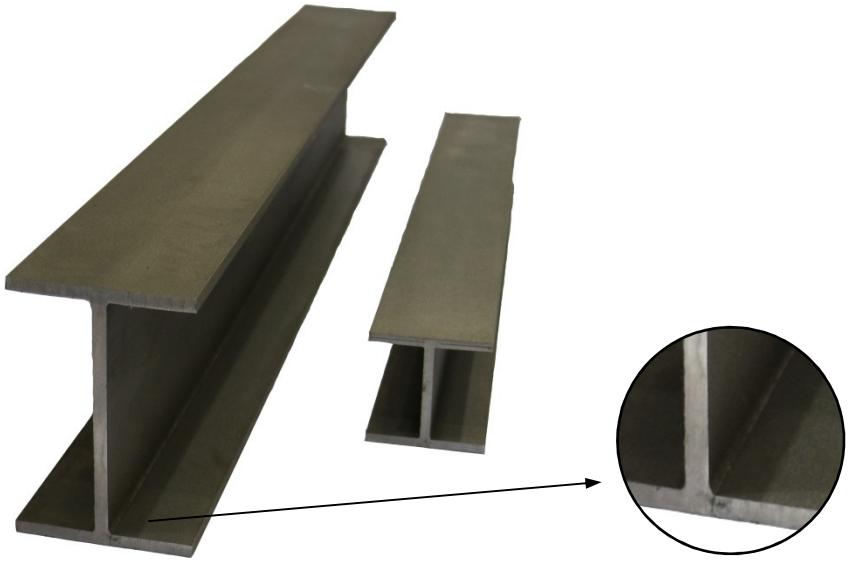

Fig. 1. Laser-welded test specimens.

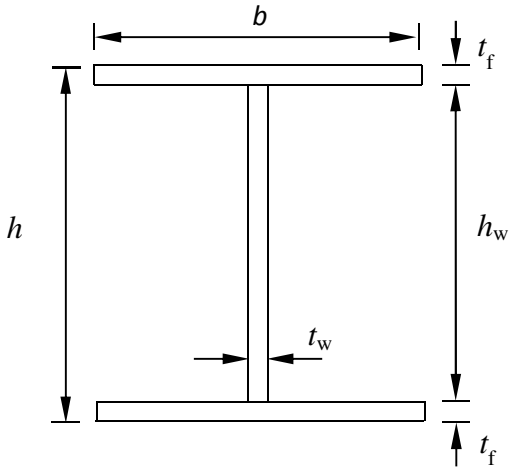

Fig. 2. Cross-section labelling system.

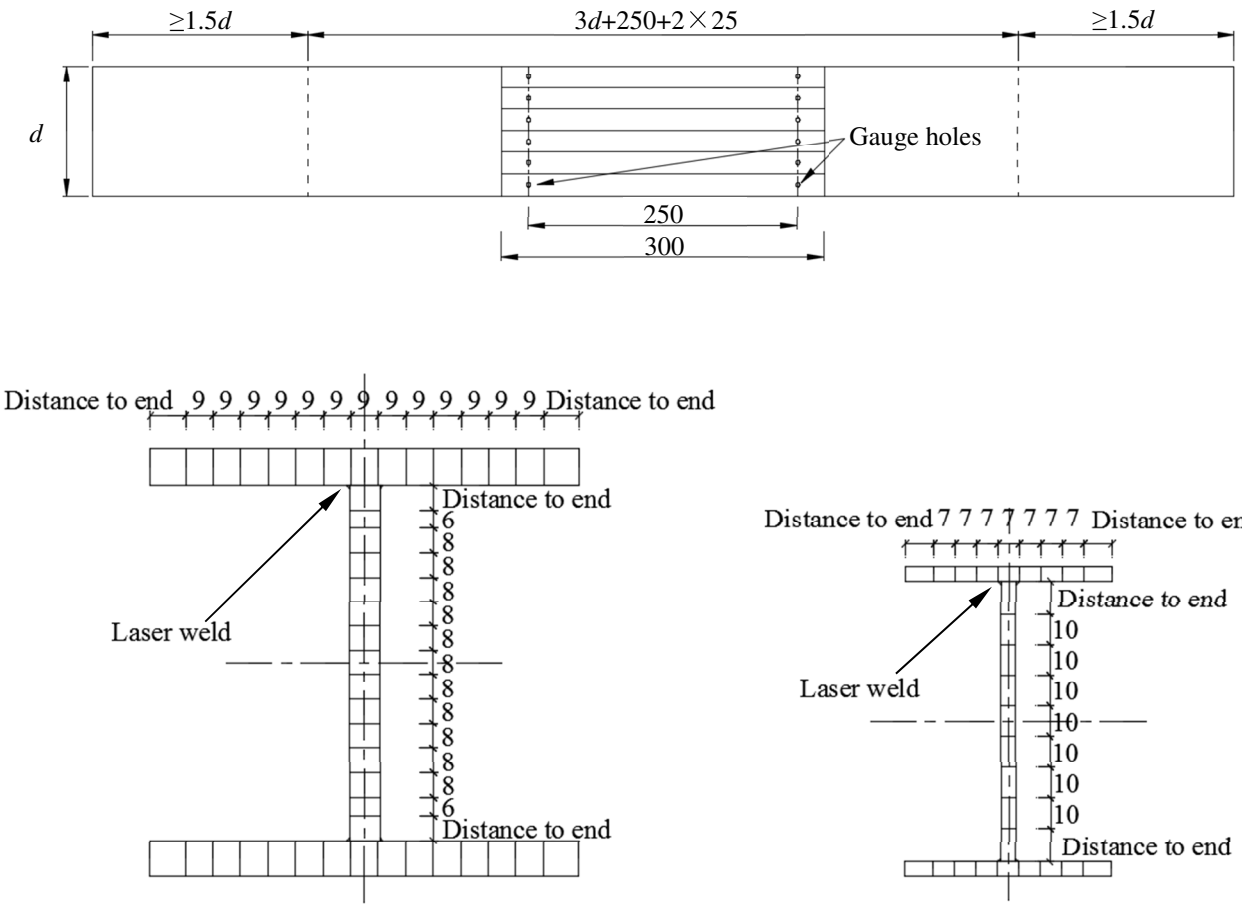

(a) I-140×140×10×12. (b) I-102×68×5×5.

Fig. 3. Setting out of I-section (a) I-140×140×10×12 and (b) I-102×68×5×5 for residual stress measurements (all dimensions in mm).

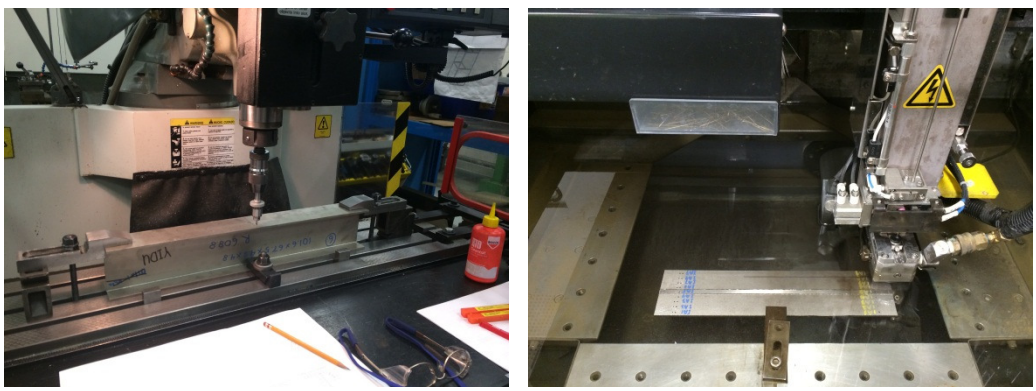

(a) CNC milling machine. (b) Wire electrical discharge machining.

Fig. 4. Drilling of gauge holes and sectioning.

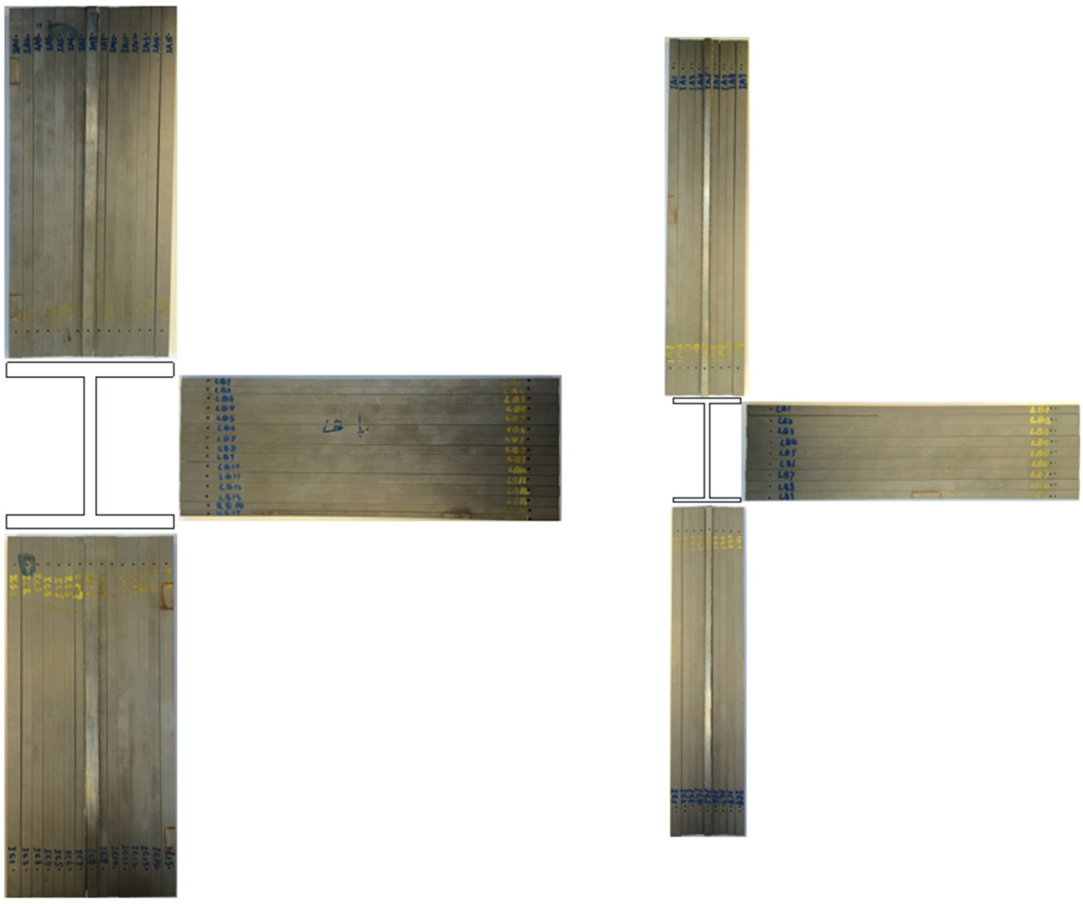

(a) I-140×140×10×12. (b) I-102×68×5×5.

Fig. 5. Sectioned residual stress test specimens.

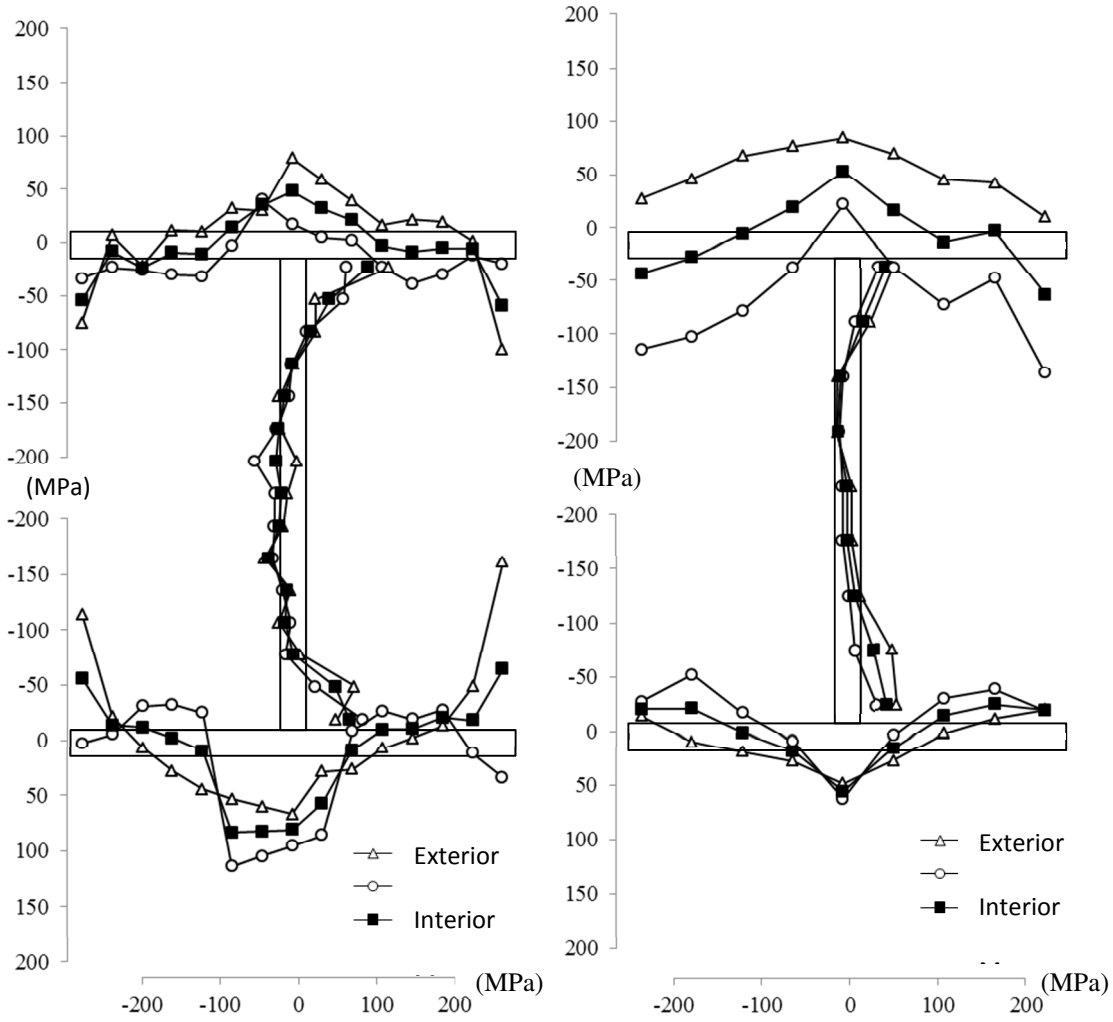

(a) I-140×140×10×12. (b) I-102×68×5×5.

Fig. 6. Measured residual stress distributions (positive = tension; negative = compression).

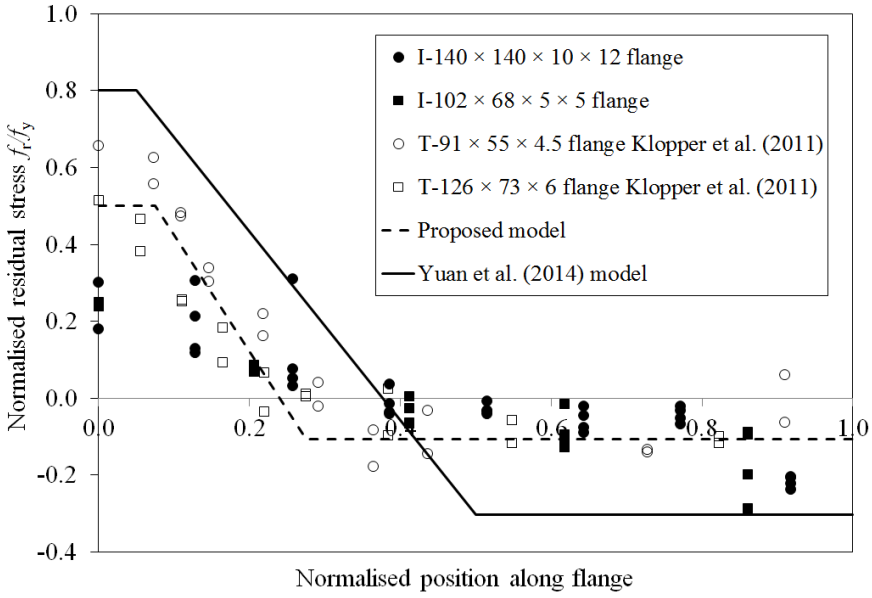

(a) Flange.

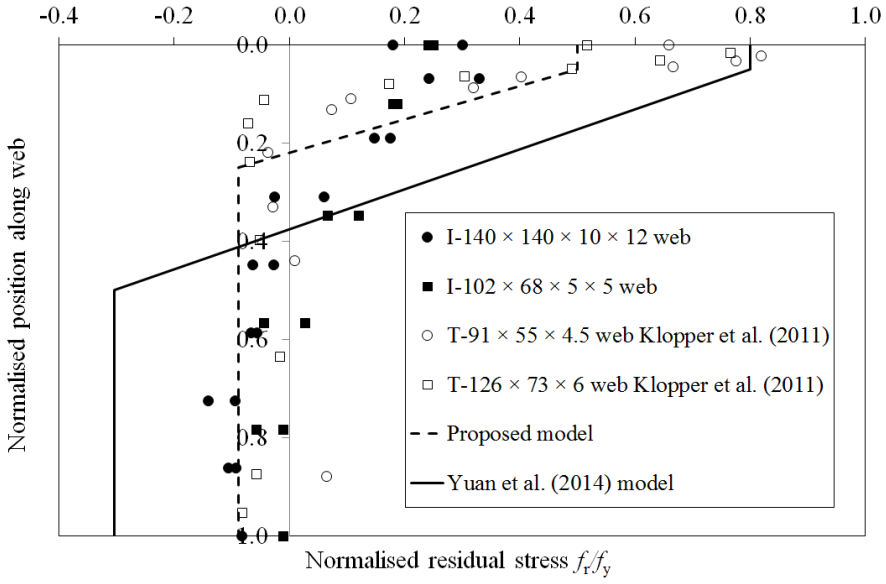

(b) Web.

Fig. 7. Comparison between measured residual stresses in laser-welded stainless steel I-sections and predictive models.

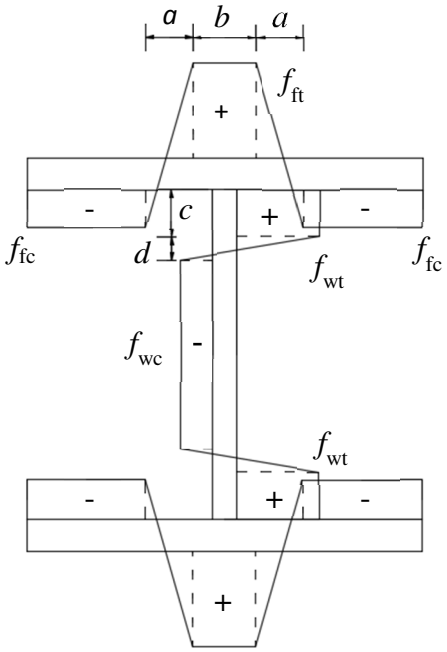

Fig. 8. General residual stress distribution for welded I-sections.

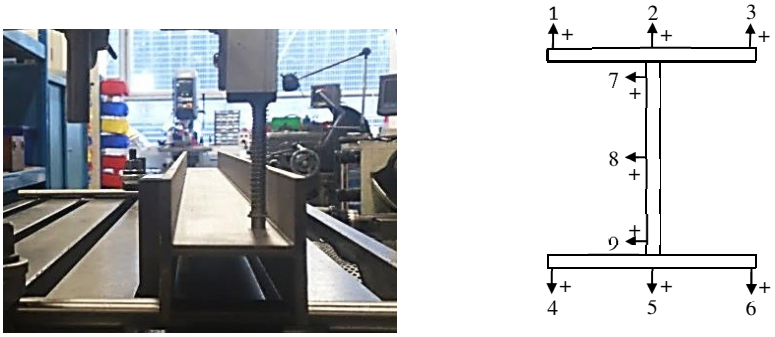

(a) Imperfection measurement setup. (b) Imperfection measurement locations.

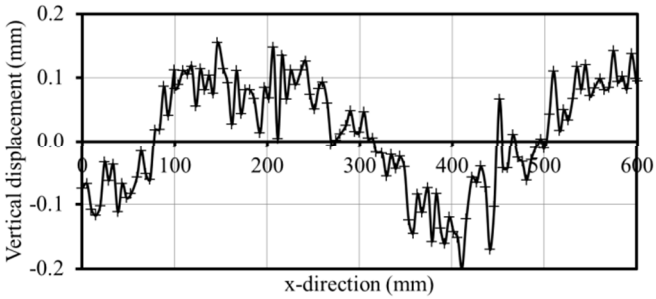

(c) Bottom flange imperfection measurement for I-102×68×5×5 cross-section.

Fig. 9. Measurement of imperfections.

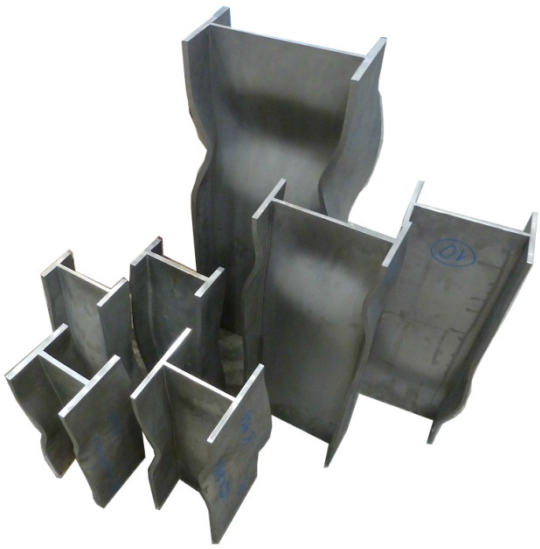

Fig. 10. Stub column failure modes.

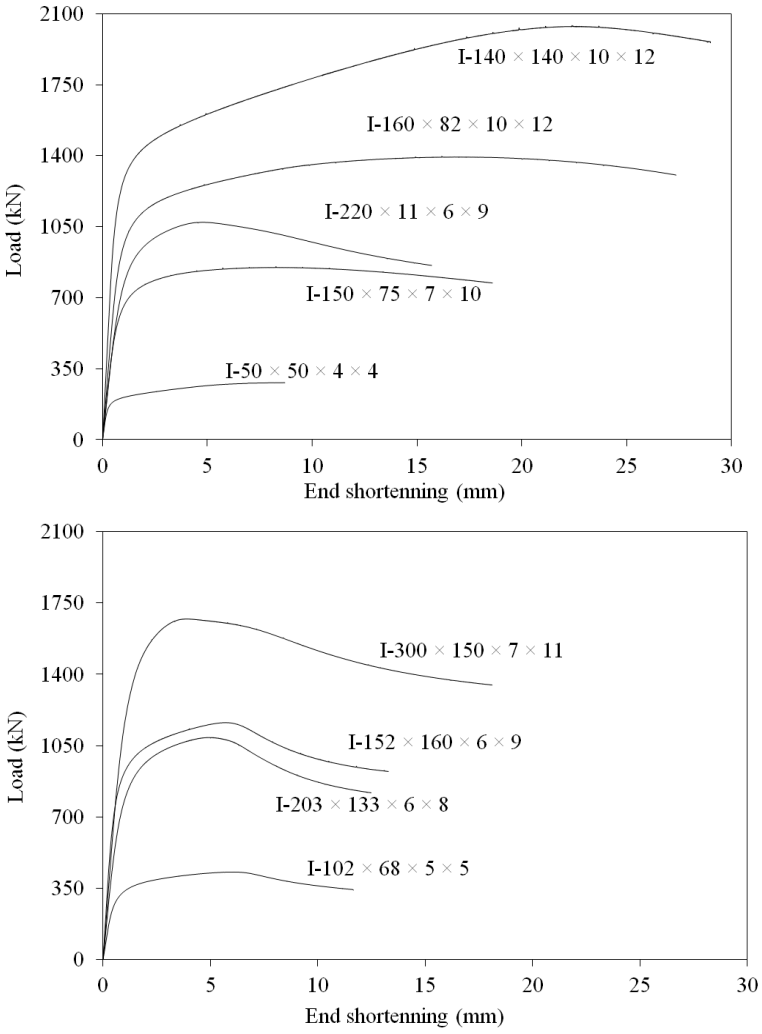

Fig. 11. Load-end shortening responses of tested stub column specimens.

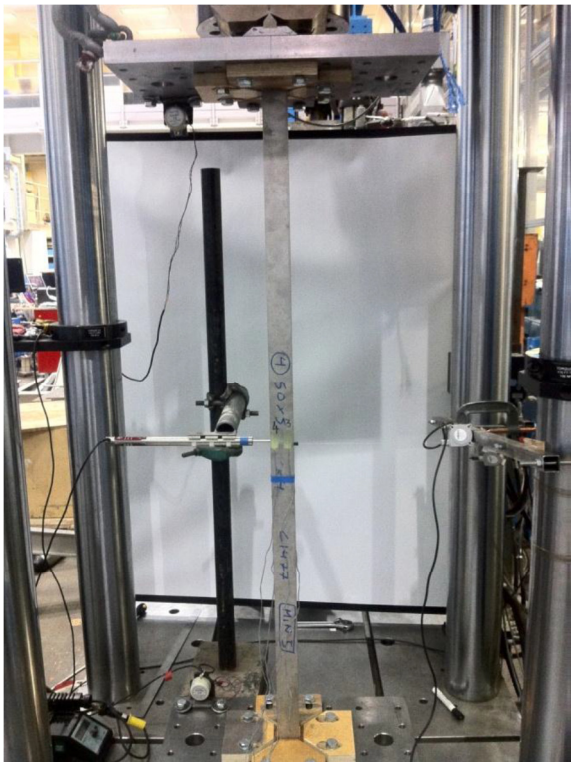

Fig. 12. Minor flexural buckling test setup.

Fig. 13. Typical failure modes for minor flexural buckling.

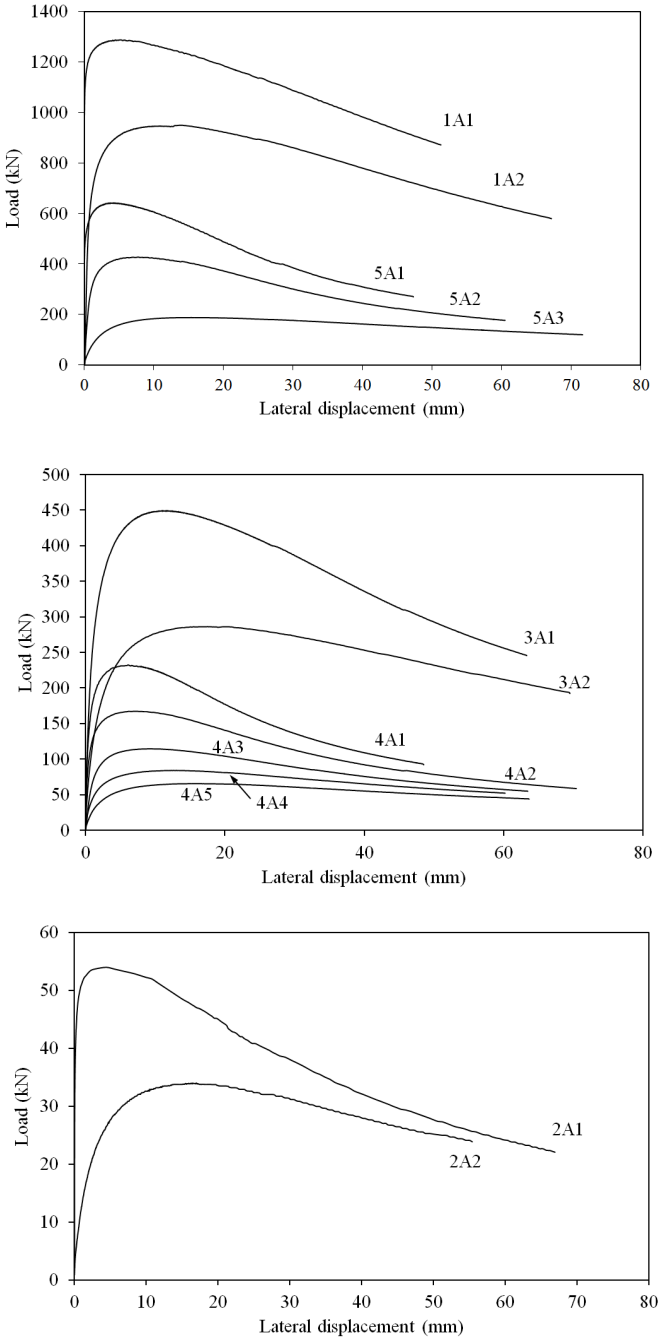

Fig. 14. Load-lateral displacement curves for minor flexural buckling tests.

Fig. 15. Major flexural buckling test setup.

Fig. 16. Major flexural buckling failure modes.

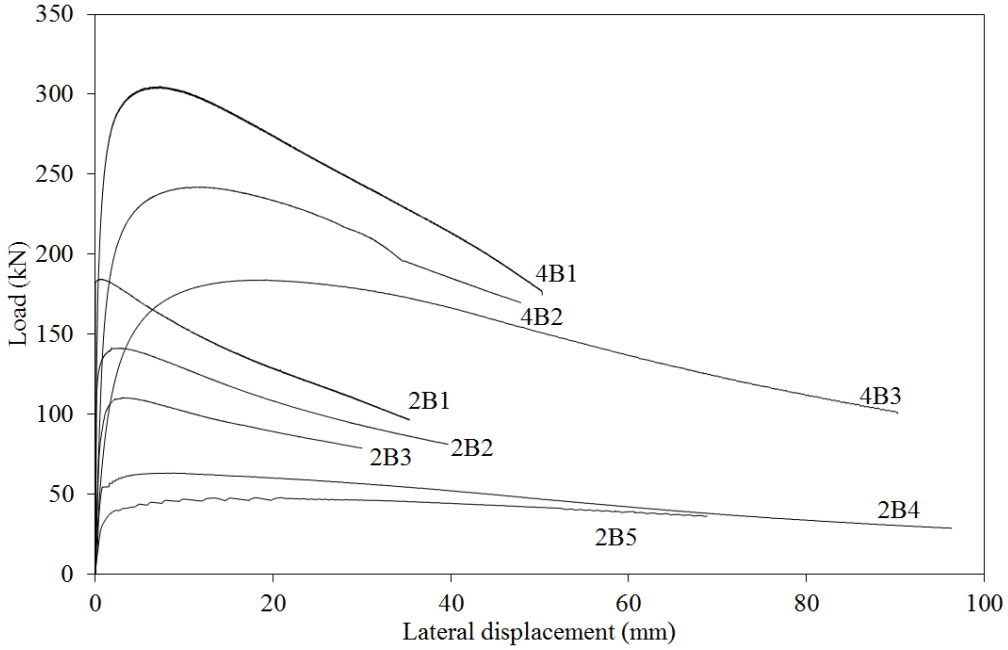

Fig. 17. Load-lateral displacement curves for major flexural buckling tests.

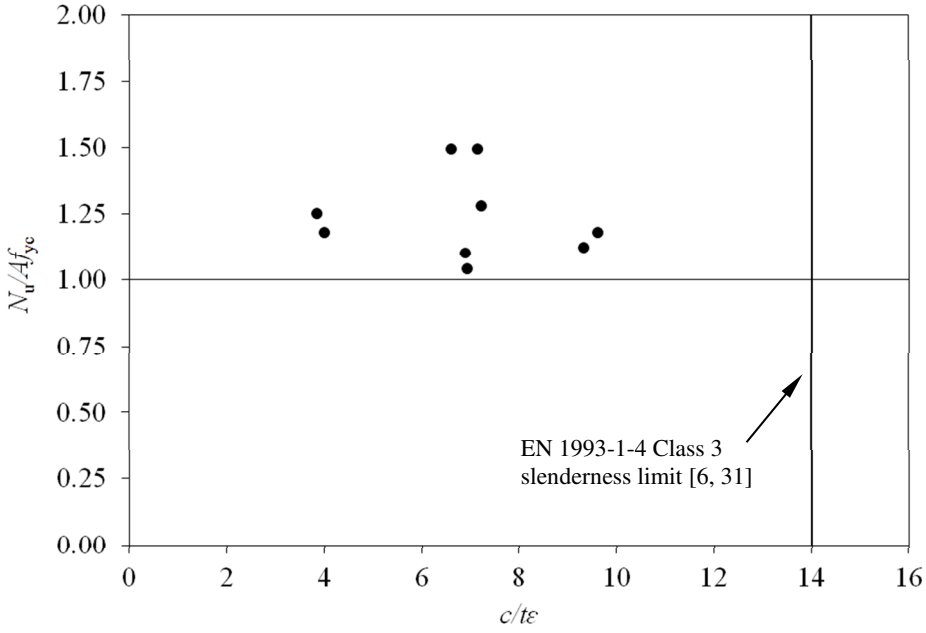

(a) Outstand elements.

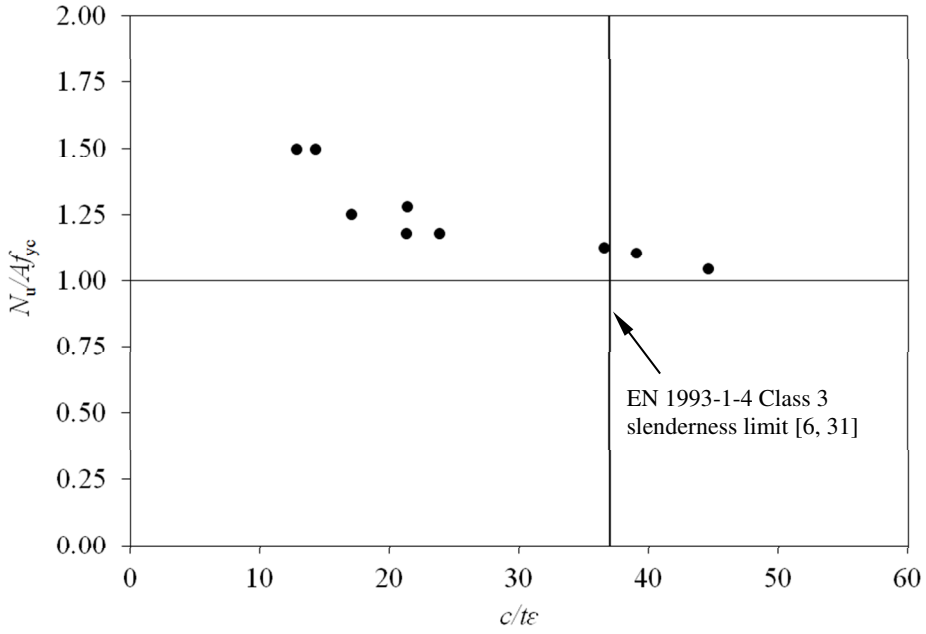

(b) Internal elements.

Fig. 18. Assessment of Class 3 limit.

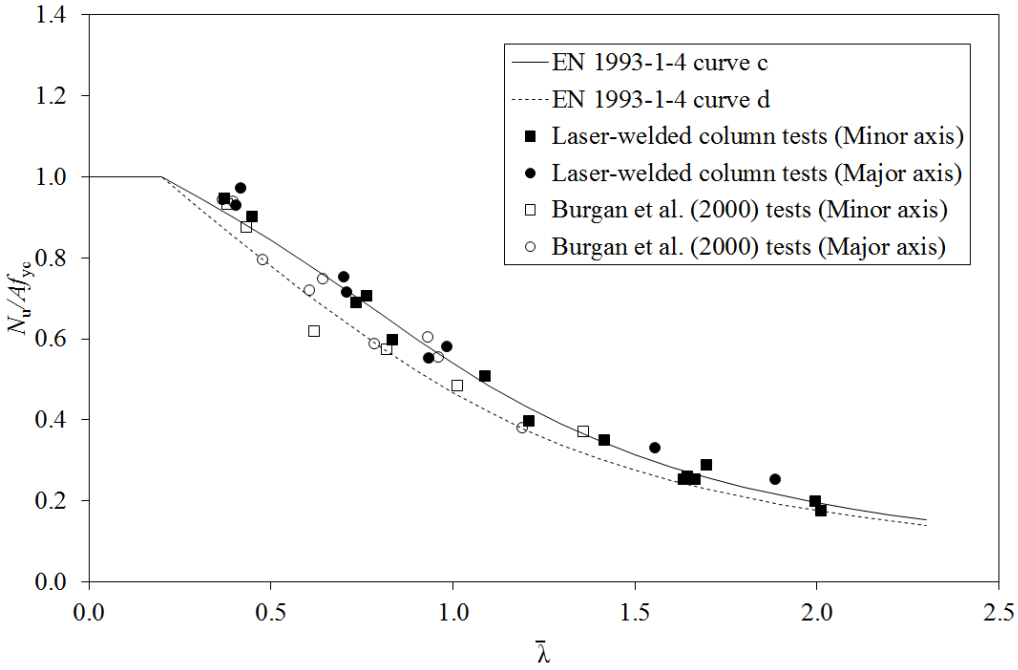

Fig. 19. Assessment of codified buckling curves for welded and laser-welded stainless steel I-sections.

Table 1 Chemical composition from mill certificates.

Specimen	Material grade	C (%)	Si (%)	Mn (%)	P (%)	S (%)	Cr (%)	Ni (%)	N (%)	Mo (%)	Ti (%)
I-50×50×4×4	1.4307	0.026	0.37	1.41	0.032	0.002	18.04	8.00	0.062	-	-
I-102×68×5×5	1.4571	0.022	0.38	1.12	0.027	0.007	16.77	11.05	0.012	2.06	0.28
I-140×140×10×12-W	1.4307	0.021	0.47	1.50	0.037	0.003	18.10	8.07	0.066	-	-
I-140×140×10×12-F	1.4307	0.023	0.45	1.54	0.026	0.001	18.08	8.00	0.067	-	-
I-150×75×7×10-W	1.4404	0.022	0.45	1.08	0.029	0.003	16.59	10.54	0.019	2.01	-
I-150×75×7×10-F	1.4404	0.020	0.39	1.07	0.027	0.003	16.64	10.59	0.010	2.02	-
I-152×160×6×9-W	1.4571	0.026	0.72	1.41	0.022	0.001	16.80	11.20	0.160	2.13	0.40
I-152×160×6×9-F	1.4571	0.029	0.50	1.09	0.026	0.004	16.59	11.04	-	2.04	0.35
I-160×82×10×12-W	1.4307	0.025	0.43	1.33	0.033	0.003	18.17	8.06	0.055	-	-
I-160×82×10×12-F	1.4307	0.017	0.39	1.82	0.029	0.001	18.24	8.13	0.044	-	-
I-203×133×6×8-W	1.4404	0.021	0.40	1.10	0.030	0.003	16.66	10.57	0.008	2.01	-
I-203×133×6×8-F	1.4404	0.024	0.39	1.17	0.030	0.004	16.61	10.54	0.009	2.02	-
I-220×110×6×9-W	1.4307	0.025	0.40	1.40	0.030	0.002	18.00	8.00	0.068	-	-
I-220×110×6×9-F	1.4307	0.023	0.46	1.40	0.030	0.003	18.02	8.01	0.072	-	-
I-300×150×7×11-W	1.4571	0.025	0.43	1.19	0.026	0.002	16.52	10.51	0.010	2.01	0.32
I-300×150×7×11-F	1.4571	0.021	0.42	1.11	0.028	0.002	16.59	10.51	0.011	2.01	0.42

Table 2 Material properties from mill certificates.

Specimen	$f_{y,mill}$	$f_{1.0,mill}$	$f_{u,mill}$	$\varepsilon_{f,mill}$

	(N/mm^2)	(N/mm^2)	(N/mm^2)	(%)
I-50×50×4×4	290	327	652	58
I-102×68×5×5	283	325	581	52
I-140×140×10×12-W	385	429	656	52
I-140×140×10×12-F	349	382	634	52
I-150×75×7×10-W	311	345	564	53
I-150×75×7×10-F	278	312	575	53
I-152×160× 6 × 9-W	316	349	595	46
I-152 ×160×6×9-F	305	331	553	53
I-160×82×10×12-W	353	389	623	57
I-160×82×10×12-F	305	354	607	55
I-203×133×6×8-W	292	328	575	55
I-203×133×6×8-F	279	320	581	54
I-220×110×6×9-W	331	371	641	55
I-220×110×6×9-F	290	327	615	57
I-300×150×7×11-W	398	433	599	45
I-300×150×7×11-F	297	328	585	55

Table 3 Measured material properties from tensile coupon tests.

Specimen	t (mm)	E (N/mm^2)	f_y (N/mm^2)	$f_{1.0}$ (N/mm^2)	f_u (N/mm^2)	ε_u (%)	ε_f (%)	Compound R-O coefficients		
								n	$n_{0.2,1.0}$	$n_{0.2,u}$
I-50×50×4×4	4.01	190700	270	361	694	61	73	4.0	3.2	3.0
I-102×68×5×5	4.99	186800	222	331	580	50	64	3.2	3.9	3.8
I-140×140×10×12-W	9.69	186800	260	312	617	55	66	7.0	2.2	2.5
I-140×140×10×12-F	11.96	193700	272	328	615	50	64	7.1	2.4	2.6
I-150×75×7×10-W	6.88	197300	274	344	596	58	68	5.0	3.1	3.0
I-150×75×7×10-F	9.88	197200	267	323	560	50	66	5.0	2.7	2.7
I-152×160×6×9-W	6.18	191400	272	349	586	50	65	5.2	3.3	3.2
I-152×160×6×9-F	8.68	204700	227	287	561	52	67	6.0	2.6	2.8
I-160×82×10×12-W	9.81	198500	264	341	618	53	64	5.2	3.0	3.1
I-160×82×10×12-F	11.69	197500	286	342	619	52	65	7.5	2.7	2.5
I-203×133×6×8-W	5.90	192500	251	320	576	55	67	4.1	2.9	2.9
I-203×133×6×8-F	7.85	192500	281	365	597	47	64	4.2	3.4	3.3
I-220×110×6×9-W	6.02	193000	275	349	670	61	71	6.0	2.9	2.8
I-220×110×6×9-F	8.91	197200	292	355	671	55	65	6.2	2.5	2.6
I-300×150×7×11-W	6.89	200600	237	306	581	55	69	5.6	2.9	3.0
I-300×150×7×11-F	11.87	196500	290	346	589	45	64	5.8	2.7	2.6

Table 4 Measured geometric dimensions for residual stress test specimens.

Specimen	h (mm)	b (mm)	t_w (mm)	t_f (mm)	c_f/t_f	h_w/t_w

I-140×140×10×12	140.67	139.91	9.71	11.89	5.48	12.04
I-102×68×5×5	101.80	68.00	5.11	5.05	6.23	18.95

Table 5 Summary of peak residual stresses for the two tested cross-sections.

Specimen	f_{ft}/f_y	f_{fc}/f_y	f_{wt}/f_y	f_{wc}/f_y
I-140×140×10×12	0.24	-0.22	0.29	-0.14
I-102×68×5×5	0.25	-0.17	0.18	-0.06
Mean	0.25	-0.19	0.23	-0.10
Maximum	0.25	-0.22	0.29	-0.14

Table 6 Parameters in predictive models for welded I-sections.

Predictive model	$f_{ft}=f_{wt}$	$f_{fc}=f_{wc}$	a	b	c	d
Proposed model	$0.5f_y$	From equilibrium	$0.1b_f$	$0.075b_f$	$0.025h_w$	$0.05h_w$
Yuan et al. [17]	$0.8f_y$	From equilibrium	$0.225b_f$	$0.05b_f$	$0.025h_w$	$0.225h_w$
ECCS [24]	f_y	$0.25f_y$	$0.05b_f$	$0.15b_f$	$0.075h_w$	$0.05h_w$
BSK 99 [25]	$0.5f_y$	From equilibrium	$0.75t_f$	$1.5t_f$	$1.5t_w$	$1.5t_w$

Table 7 Measured geometry and key experimental results for tested I-section stub columns.

Specimen	L (mm)	h (mm)	b (mm)	t_w (mm)	t_f (mm)	w_0 (mm)	$w_{0,tol}$ (mm)	f_{yc} (N/mm^2)	N_u (kN)	δ_u (mm)	N_u /Af_{yc}
I-50×50×4×4	150.29	50.33	50.49	3.99	3.91	0.23	0.43	332	281.1	8.69	1.50
I-102×68×5×5	304.72	101.80	68.00	5.01	5.11	0.22	0.68	291	429.7	6.05	1.28
I-140×140×10×12	420.32	139.78	140.78	9.71	11.82	1.30	1.16	306	2042.2	22.40	1.50
I-150×75×7×10	450.09	150.46	75.83	7.05	9.90	0.16	0.76	298	854.0	8.27	1.18
I-152×160×6×9	456.12	152.28	160.57	6.18	8.79	0.34	1.35	270	1163.2	5.67	1.18
I-160×82×10×12	480.19	159.95	83.24	9.79	11.72	0.16	0.83	339	1397.5	16.19	1.25
I-203×133×6×8	612.09	205.08	133.90	5.90	7.83	0.11	1.34	301	1090.3	4.85	1.13
I-220×110×6×9	660.00	219.60	110.41	6.07	8.91	0.15	1.10	304	1071.8	4.65	1.10
I-300×150×7×11	840.00	295.16	150.52	6.92	11.81	0.20	1.51	295	1672.4	3.86	1.04

Table 8 Geometry of minor axis buckling test specimens.

Cross-section	Specimen ID	Buckling length L (mm)	h (mm)	b (mm)	t_w (mm)	t_f (mm)	Global imperfection v_0 (mm)	Total eccentricity (v_0+e_0) (mm)
I-140×140×10×12	1A1	1030.1	139.73	140.64	9.73	11.88	0.28	0.35
I-140×140×10×12	1A2	2032.1	140.17	140.62	9.86	11.91	0.29	1.42
I-50×50×4×4	2A1	1631.1	50.43	50.53	4.03	4.05	0.38	0.53
I-50×50×4×4	2A2	1931.1	50.68	50.54	4.00	4.02	0.70	1.52
I-160×82×10×12	3A1	1730.1	160.86	83.23	9.88	11.84	0.15	1.22
I-160×82×10×12	3A2	2323.1	160.49	82.80	9.88	11.85	0.43	1.67
I-102×68×5×5	4A1	931.1	101.56	67.96	5.03	5.00	0.11	0.80
I-102×68×5×5	4A2	1330.1	101.51	67.96	5.02	5.04	0.08	0.65
I-102×68×5×5	4A3	1730.1	101.80	67.99	5.03	5.02	0.33	1.05

I-102×68×5×5	4A4	2030.1	101.76	67.88	4.99	4.98	0.33	1.85
I-102×68×5×5	4A5	2430.1	101.78	67.83	5.01	4.99	0.27	1.60
I-150×75×7×10	5A1	634.1	150.18	75.87	6.91	9.81	0.02	0.55
I-150×75×7×10	5A2	1361.1	150.22	75.91	6.91	9.85	0.05	1.35
I-150×75×7×10	5A3	2331.1	150.34	75.90	6.87	9.86	0.50	1.44

Table 9 Key experimental results of minor axis buckling test specimens.

Cross-section	Specimen ID	Buckling length L (mm)	Ultimate load N_u (kN)	Lateral displacement at N_u (mm)	Average end rotation at N_u (°)
I-140×140×10×12	1A1	1030.1	1294.6	7.93	1.48
I-140×140×10×12	1A2	2032.1	950.6	14.08	1.40
I-50×50×4×4	2A1	1631.1	56.0	4.41	0.50
I-50×50×4×4	2A2	1931.1	33.9	16.28	1.51
I-160×82×10×12	3A1	1730.1	449.5	11.02	1.20
I-160×82×10×12	3A2	2323.1	286.5	17.50	1.52
I-102×68×5×5	4A1	931.1	234.4	5.54	1.28
I-102×68×5×5	4A2	1330.1	169.0	7.49	1.00
I-102×68×5×5	4A3	1730.1	117.2	9.37	1.03
I-102×68×5×5	4A4	2030.1	84.3	13.07	1.38
I-102×68×5×5	4A5	2430.1	66.7	15.89	1.17
I-150×75×7×10	5A1	634.1	642.7	4.35	1.19
I-150×75×7×10	5A2	1181.1	427.4	7.77	1.19
I-150×75×7×10	5A3	2331.1	188.3	15.90	1.21

Table 10 Geometry of major axis buckling test specimens.

Cross-section	Specimen ID	Buckling length L (mm)	h (mm)	b (mm)	t_w (mm)	t_f (mm)	Global imperfection v_0 (mm)	Total eccentricity (v_0+e_0) (mm)
I-50×50×4×4	2B1	680.1	51.00	50.56	3.99	3.93	0.25	1.05
I-50×50×4×4	2B2	1130.1	50.59	50.60	4.04	3.86	0.50	1.90
I-50×50×4×4	2B3	1580.1	50.28	50.32	3.99	3.98	0.75	2.15
I-50×50×4×4	2B4	2530.1	50.90	50.55	4.01	3.94	3.00	3.00
I-50×50×4×4	2B5	3030.1	50.21	50.55	4.00	3.91	0.50	3.40
I-102×68×5×5	4B1	1330.1	101.91	67.51	4.99	4.94	0.25	1.05
I-102×68×5×5	4B2	2330.1	102.37	67.94	5.21	5.01	0.25	3.15
I-102×68×5×5	4B3	3080.1	102.11	67.93	5.04	5.01	1.00	3.90

Table 11 Key experimental results of major axis buckling test specimens.

Cross-section	Specimen ID	Buckling length L (mm)	Ultimate load N_u (kN)	Lateral displacement at N_u (mm)	Average end rotation at N_u (°)
I-50×50×4×4	2B1	680.1	184.5	0.70	0.27
I-50×50×4×4	2B2	1130.1	141.4	1.80	0.29
I-50×50×4×4	2B3	1580.1	110.4	3.10	0.23
I-50×50×4×4	2B4	2530.1	63.2	7.98	0.08
I-50×50×4×4	2B5	3030.1	47.8	18.02	1.02
I-102×68×5×5	4B1	1330.1	304.9	7.22	0.94
I-102×68×5×5	4B2	2330.1	242.2	12.09	0.91
I-102×68×5×5	4B3	3080.1	184.0	19.12	1.07

Table 12 Assessment of EN 1993-1-4 [6] and CSM [31-35] for stub columns.

Design method	$N_{EN1993\text{-}1\text{-}4}/N_u$	N_{csm}/N_u
Mean	0.82	0.92
COV	0.12	0.08

Table 13 Assessment of codified buckling curves for welded and laser-welded I-sections.

Buckling axis	No. of tests	Buckling curve	Fabrication process	$N_{EN1993\text{-}1\text{-}4}/N_u$	
				Mean	COV
Minor	6	Curve d	Welded [37]	0.96	0.09
	14	Curve d	Laser-welded	0.90	0.06
Major	9	Curve c	Welded [37]	1.00	0.04
	8	Curve c	Laser-welded	0.95	0.07